SUPPLEMENTARY INFORMATION FOR

The Potential of Singlet Fission Photon Multipliers as an Alternative to Silicon-Based Tandem Solar Cells

Moritz H. Futscher[1], Akshay Rao[2] and Bruno Ehrler[1]*

1. Center for Nanophotonics, AMOLF, Science Park 104, 1098 XG Amsterdam, The Netherlands
2. Cavendish Laboratory, University of Cambridge, J.J. Thomson Avenue, Cambridge CB3 OHE, UK

Corresponding Author

* ehrler@amolf.nl

S1 SINGLET FISSION PHOTON MULTIPLIER MODEL

To model the modulation of the incident solar spectrum we assume that the singlet fission material absorbs everything above the energy of the singlet exciton E(S_1) as

$$\Phi = \int_{E(S_1)}^{E_{max}} \Gamma(E)\, dE$$

where Γ is the photon flux of the incident solar spectrum. Each absorbed photon generates one singlet exciton with an energy E(S_1) which converts into two triplet excitons with an energy E(T_1). The energy of the triplet excitons is then transferred into quantum dots (QD) which emit photons with an energy of E(QD) and a full width at half-maximum (fwhm) of σ_{QD} as

$$\Gamma_{\text{gain}}(E) = \frac{2\,\Phi\,\gamma}{\sqrt{2\,\pi}\,\sigma_{QD}}\, e^{-\frac{\left(E-E(QD)\right)^2}{2\,\sigma_{QD}^2}}$$

where γ is the capture parameter including the efficiency of triplet exciton yield form singlet fission (η_{SF}), the efficiency of triplet excitons diffusing and transferring their energy to QDs (η_T), the photoluminescence quantum efficiency of the QDs (η_{QD}), and the efficiency of photons emitted by the QDs reaching the silicon solar cell (η_C), i.e. $\gamma = \frac{\eta_{SF}}{2}\,\eta_T\,\eta_{QD}\,\eta_C$. In the ideal case, the capture parameter is unity. The generated photocurrent density in the bottom cell can then be calculated as

$$J_G = q \int_{E_{min}}^{E(S_1)} [\,\zeta\,\Gamma(E) + \Gamma_{\text{gain}}(E)\,]\,\text{EQE}(E)\, dE$$

where ζ is the fraction of light transmitted through the photon multiplier and EQE is the external quantum efficiency of the bottom cell to take additional optical losses such as parasitic absorption in the bottom cell contacts into account.

The current-voltage characteristic of a silicon solar cell can then be calculated following previous work as[1]

$$J(V) = J_G - J_R\left(e^{\frac{q\,(V+J\,R_S)}{k_B T}} - 1\right) - J_{NR}\left(e^{\frac{q\,(V+J\,R_S)}{k_B T}} - 1\right) - J_A\left(e^{\frac{3\,q\,(V+J\,R_S)}{2\,k_B T}} - 1\right) - \frac{V + J\,R_s}{R_{sh}}$$

where V the applied voltage, k_B the Boltzmann constant, T the temperature of the cell, R_s is the series resistance, and R_{sh} the shunt resistance. The second term of $J(V)$ corresponds to the radiative recombination current density, the third term to the nonradiative recombination current density, the fourth term to the Auger recombination current density, and the last term is due to parasitic resistances in the cell. The electroluminescent emission efficiency (η_{EL}) is calculated as[2]

$$J(V) = J_G - \frac{J_R}{\eta_{\mathrm{EL}}}\left(e^{\frac{q\,(V+JR_S)}{k_B T}} - 1\right) - \frac{V + JR_s}{R_{sh}}$$

where η_{EL} is calculated as

$$\eta_{EL} = \frac{J_R}{J_R + J_{NR} + J_A\left(1 + e^{\frac{3q(V+JR_S)}{2k_B T}}\right)^{-1}}.$$

The current-voltage characteristics of a silicon solar cell can then be fitted by including the EQE and the silicon thickness L, and adjusting the amount of nonradiative recombination J_{NR}, R_s, and R_{sh}. The current-voltage characteristics of the modeled record silicon solar cells together with the fitting parameters and its EQE is shown in Figure S1.

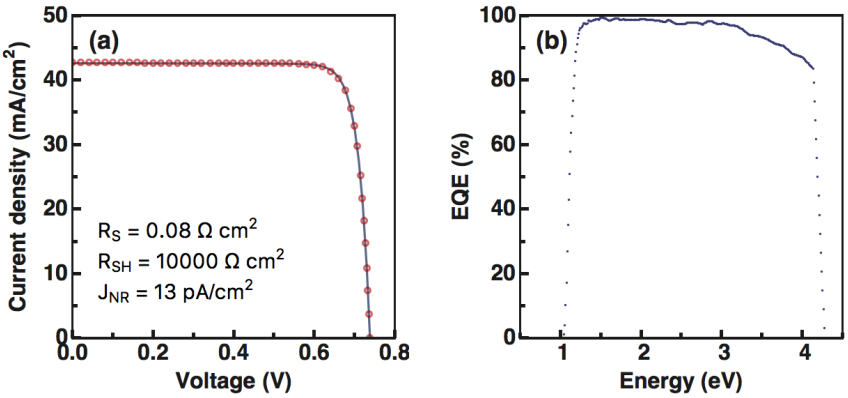

Figure S1. (a) Current–voltage characteristics of the record efficiency silicon solar cells with an area of 79 cm^2, a V_{OC} of 0.738 V, a J_{SC} of 42.65 mA/cm^2, a fill factor of 84.9%, an η_{EL} of 0.4%, and an efficiency of 26.7%.[3] The circles correspond to the measured data of the record efficiency silicon solar cell and the solid line corresponds to the fitted current-voltage characteristics. **(b)** External quantum efficiency of the record silicon solar cell used to account for optical losses.

S2 OPTICAL MODEL

Placing a photon multiplier on a silicon solar cell influences the light that reaches the silicon solar cell. However, a photon multiplier has only a few interfaces more compared to a silicon solar cell with an antireflection coating. By optimizing the cell design, most of the light can reach the silicon solar cell below the photon multiplier. Figure S2 shows transfer matrix simulations[4] of a silicon solar cell with different antireflection coatings and a photon multiplier on a silicon solar cell. Bare silicon has a high surface reflection of more than 30%. The reflection can be reduced by an antireflection coating, as shown for 70 nm SiN and 105 nm SiO_2 on 70 nm SiN. Similarly, the reflection is reduced by placing a photon multiplier consistent of a singlet fission material (in our case pentacene, 1000 nm) and quantum dots (PbS, 3 nm) on a silicon solar cell. By placing 110 nm of SiN between the silicon cell and the photon multiplier, the reflection is reduced to less than 7% above the singlet fission band gap. This value is likely to be improved by optimizing the cell design. These simulations are

furthermore based on flat surfaces. Texturing the surfaces would further reduce the reflection significantly.

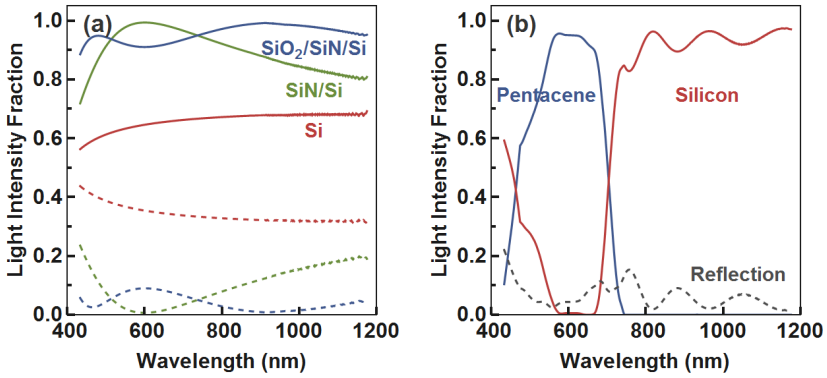

Figure S2. Transfer matrix simulations of **(a)** a silicon solar cell using different antireflection coatings and **(b)** a silicon solar cell with a photon multiplier on top. The continuous and the dashed lines in (a) correspond to the absorption and the reflection, respectively. The photon multiplier is assumed to consist of 1000 nm Pentacene, 3 nm of PbS quantum dots, and 110 nm SiN. The n and k values for this simulation are taken from: [5–8].

To calculate the amount of light absorbed by the quantum dots, we estimate that the absorption of quantum dots distributed in a micron-thick singlet fission layer, spaced by 50 nm, is equal to the absorption of 3 nm thick PbS quantum dot layer. The absorption above the band gap of silicon can then be calculated using the Lambert–Beer law as

$$A = 1 - \int_{E_{G,Si}}^{E_{max}} e^{\frac{-4\pi k(\lambda)}{3\ nm}}\, d\lambda$$

resulting in an absorption of 0.44%.

Assuming that the quantum dots are isotropic emitters embedded in the singlet fission layer, part of the emission is lost due to out-coupling from the singlet fission layer to air, referred to as light within the escape cone. The fraction of light within the escape cone can be approximated as

$$\frac{\Omega}{4\pi} = \frac{1}{2}(1 - \cos\theta)$$

where Ω is the solid angle of a cone and θ is the critical angle for total internal reflection. If the singlet fission material has a refractive index of 1.7 or higher, less than 10% of the light emitted by the quantum dots is within the escape cone.

S3 TANDEM SOLAR CELL MODEL

To model a perovskite solar cell with an ideal band gap for a tandem solar cell in combination with silicon, we first fit the current-voltage characteristic of the current record perovskite solar with a band gap of 1.49 eV, an area of 0.09 cm^2, and an efficiency of 22.7%.[9] We calculate the current-voltage characteristic of a perovskite solar cell following previous work as[1]

$$J(V) = J_G - J_R\left(e^{\frac{q(V+JR_S)}{k_BT}} - 1\right) - J_{NR}\left(e^{\frac{q(V+JR_S)}{2k_BT}} - 1\right) - \frac{V + JR_s}{R_{sh}}.$$

The electroluminescent emission efficiency for the perovskite cell is calculated as

$$\eta_{EL} = \frac{J_R}{J_R + J_{NR}(V)\left(1 + e^{\frac{q(V+JR_S)}{2k_BT}}\right)^{-1}}.$$

The current-voltage characteristics of a perovskite solar cell can then be modeled by including the EQE and adjusting the amount of nonradiative recombination J_{NR}, R_s, and R_{sh}. The current-voltage characteristics of the modeled record perovskite solar cells together with the fitting parameters and its EQE is shown in Figure S3**.**

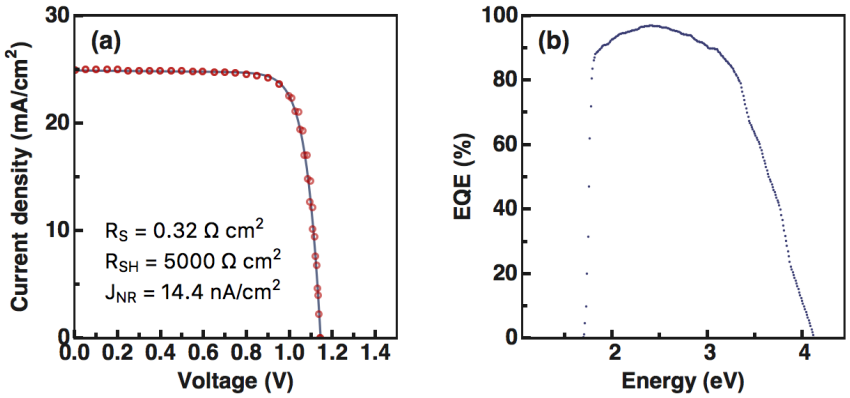

Figure S3. (a) Current−voltage characteristics of the record efficiency perovskite solar cells with a band gap of 1.49 eV, an area of 0.09 cm^2, a V_{OC} of 1.144 V, a J_{SC} of 24.91 mA/cm^2, a fill factor of 79.6%, an η_{EL} of 0.15% at maximum power point (MPP), and an efficiency of 22.7%.[9] The circles correspond to the measured data of the record efficiency perovskite solar cell and the solid line corresponds to the modeled current-voltage characteristics. **(b)** External quantum efficiency of the record perovskite solar cell used to account for optical losses.

To optimize for maximum perovskite/silicon tandem solar cell efficiency, we change the band gap of the perovskite solar cell artificially by scaling the EQE of the record perovskite solar cell in energy until current matching between the perovskite top cell and the silicon bottom cell is achieved while keeping the parasitic resistances and the electroluminescent emission efficiency constant. The modeled perovskite solar cell then has a band gap of 1.68 eV and an efficiency of 20.9%. The current-voltage characteristics of the modeled perovskite solar cell with an ideal band gap together with the fitting parameters and its EQE is shown in Figure S4.

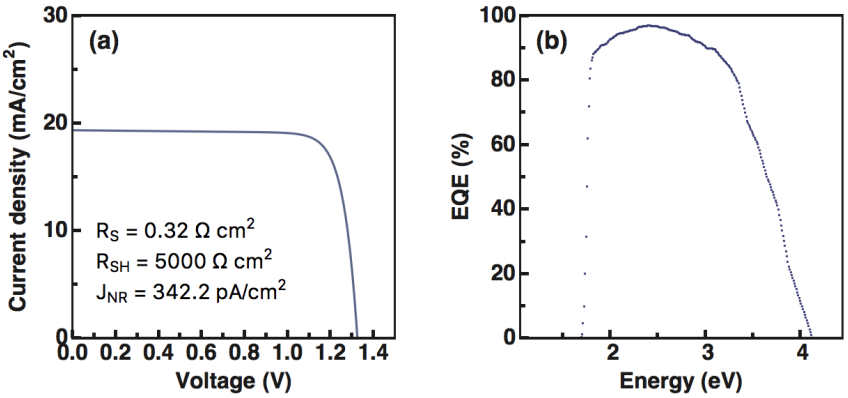

Figure S4. (a) Current–voltage characteristics and **(b)** external quantum efficiency of the perovskite solar cells with a band gap of 1.68 eV, a V_{OC} of 1.325 V, a J_{SC} of 19.36 mA/cm^2, a fill factor of 81.5%, an η_{EL} of 0.15% at MPP, and an efficiency of 20.9% used to model the perovskite/silicon tandem solar cell.

To model the perovskite/silicon tandem solar cell we apply modifications to the detailed-balance limit following previous work.[10] The power for the monolithic two-terminal tandem solar cell is calculated as

$$P_{out} = (V_{Perovskite} + V_{Silicon})J$$

The conversion efficiency for perovskite/silicon tandem solar cells is then given by

$$\eta = Max\left(\frac{P_{out}(V)}{P_{sun}}\right)$$

where P_{sun} is the power of the incident solar spectrum. Optical losses are included by fitting a Gaussian distribution to the onset of the EQE spectra of the perovskite cell. 10% of the light with an energy below the Gaussian distribution is assumed to be uniformly absorbed by parasitic absorption in the perovskite contacts. The current-voltage characteristics of the modeled perovskite/silicon tandem solar cells together the EQE of the optimistic perovskite and the record silicon subcell is shown in Figure S5.

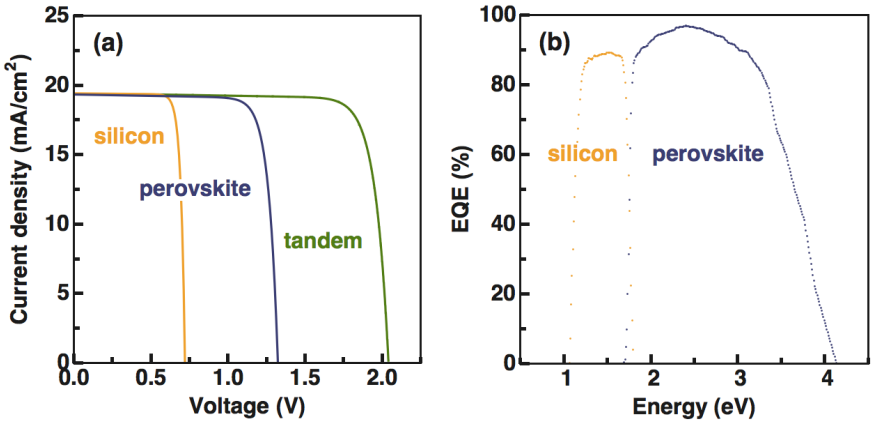

Figure S5. (a) Current-voltage characteristics and **(b)** external quantum efficiency of the modeled monolithic two-terminal perovskite/silicon tandem solar cell with an efficiency of 32.7% together with its subcells.

S4 MODELED SILICON SOLAR CELLS

To simulate the performance of a photon multiplier and a tandem solar cell as a function of the silicon solar cell efficiency, we fit our model to a variety of certified silicon solar cells. The parameters of the modeled silicon solar cells are shown in Table S1. Cell 1 to cell 13 are modeled after previous record silicon solar cells including monocrystalline and polycrystalline silicon solar cell, with cell 13 being the current record silicon solar cell. Cell 14 and 15 are hypothetical, idealized cells. Cell 14 and cell 15 both assume an ideal EQE of 100% above the silicon band gap, and cell 15 additionally assumes no Auger recombination.

To optimize for maximum efficiency of the photon multiplier and the tandem solar cell, we optimize the band gap of the perovskite solar cell, the absorption edge of the singlet fission material $E(S_1)$, and E(QD) for each modeled silicon solar cell. The parameters for the optimistic and the realistic photon multiplier for each silicon solar cell are shown in Table S2 and Table S3, respectively. The parameters for the optimized perovskite solar cells for each silicon solar cell are shown in Table S4. The effect of fwhm on the efficiency is shown in Table S5 and Table S6. Table S7, Table S8, and Table S9 furthermore show the fitting parameters to Figure 4 in the main text.

Table S1. Summary of modeled silicon solar cells calculated at standard test conditions (AM1.5G, 25 °C, 1 kWh/m^2). Thicknesses of active material L marked with an asterisk are estimates.

Cell	Source	V_{OC} (V)	J_{SC} (mA/cm^2)	FF (%)	η (%)	R_S (Ωcm^2)	R_{SH} (Ωcm^2)	J_{NR} (pA/cm^2)	η_{EL} (‰)	L (μm)
1	[11]	0.648	36.29	75.7	17.8	1.48	1800	400	0.13	170
2	[12]	0.638	37.19	76.7	18.2	1.15	1300	591	0.09	180*
3	[13]	0.650	37.38	76.2	18.5	1.35	1800	386	0.13	180
4	[14]	0.649	37.50	78.9	19.2	0.82	1800	400	0.13	190
5	[15]	0.692	36.41	77.4	19.5	1.28	1200	72	0.71	180*
6	[16]	0.657	38.10	79.5	19.9	0.73	2000	297	0.17	180*
7	[17]	0.663	39.03	80.3	20.8	0.59	2000	241	0.21	190
8	[18]	0.674	41.07	80.5	22.3	0.60	3000	166	0.31	195
9	[15]	0.742	39.31	81.6	23.8	0.67	2000	10	4.98	150
10	[16]	0.736	41.39	80.1	24.4	0.75	800	13	3.84	200
11	[19]	0.740	41.81	82.7	25.6	0.47	4000	12	4.4	150
12	[16]	0.744	42.26	83.8	26.4	0.31	6000	10	5.3	200
13	[20]	0.738	42.65	84.9	26.7	0.08	10000	13	4.0	200
14	-	0.776	43.61	88.3	29.9	0.01	10000	1	69.9	200
15	-	0.814	43.61	86.1	30.6	0.01	10000	1	69.9	200

Table S2. Summary of parameters for the optimistic singlet fission photon multiplier and the resulting solar cell for each silicon bottom cell calculated at standard test conditions. The optimistic case assumes 200 meV entropy gain, 3% parasitic absorption losses below the singlet fission band gap, capture losses of 5%, and a fwhm for the QD emission of 30 meV.

Cell	$E(S_1)$ (eV)	E(QD) (eV)	V_{OC} (V)	J_{SC} (mA/cm^2)	FF (%)	η (%)
1	2.20	1.20	0.652	43.15	74.5	21.0
2	2.26	1.23	0.642	42.91	76.0	20.9
3	2.28	1.24	0.654	43.51	75.3	21.4
4	2.32	1.26	0.652	43.14	78.4	22.1
5	2.3	1.25	0.695	41.90	76.8	22.4
6	2.32	1.26	0.660	43.60	79.10	22.8
7	2.32	1.26	0.666	44.50	80.0	23.7
8	2.26	1.23	0.678	47.76	80.1	25.9
9	2.30	1.25	0.754	45.05	81.3	27.3
10	2.26	1.23	0.740	47.68	79.8	28.1
11	2.28	1.24	0.744	48.48	82.5	29.7
12	2.26	1.23	0.748	49.22	83.7	30.8
13	2.24	1.22	0.742	49.63	85.0	31.3
14	2.18	1.19	0.780	52.29	88.4	36.0
15	2.18	1.19	0.819	52.29	86.2	36.9

Table S3. Summary of parameters for the realistic singlet fission photon multiplier and the resulting solar cell for each silicon bottom cell calculated at standard test conditions. The realistic case assumes 100 meV entropy gain, 5% parasitic absorption losses below the singlet fission band gap, capture losses of 15%, and a fwhm for the QD emission of 30 meV.

Cell	$E(S_1)$ (eV)	E(QD) (eV)	V_{OC} (V)	J_{SC} (mA/cm^2)	FF (%)	η (%)
1	2.30	1.20	0.651	40.04	75.1	19.5
2	2.36	1.23	0.640	40.06	76.4	19.6
3	2.38	1.24	0.652	40.61	75.7	20.0
4	2.42	1.26	0.651	40.29	78.6	20.6
5	2.40	1.25	0.694	39.14	77.1	20.9
6	2.42	1.26	0.659	40.72	79.3	21.3
7	2.42	1.26	0.664	41.60	80.2	22.1
8	2.36	1.23	0.676	44.43	80.3	24.1
9	2.42	1.26	0.743	42.07	81.5	25.5
10	2.36	1.23	0.738	44.42	80.0	26.2
11	2.38	1.24	0.742	45.11	82.6	27.6
12	2.36	1.23	0.746	45.73	83.8	28.6
13	2.34	1.22	0.740	46.10	84.9	29.0
14	2.28	1.19	0.778	48.24	88.3	33.1
15	2.28	1.19	0.817	48.24	86.2	33.9

Table S4. Summary of the parameters for the modeled perovskite solar cell for each silicon bottom cell calculated at standard test conditions, together with the tandem solar cell efficiency. All modeled perovskite solar cells have a shunt resistance of 5000 Ω cm^2, a series resistance of 0.32 Ω cm^2, and an η_{EL} of 0.15% at MPP.

Cell	Band gap (eV)	J_{NR} (pA/cm^2)	V_{OC} (V)	J_{SC} (mA/cm^2)	FF (%)	η (%)	η_{Tandem} (%)
1	1.74	104	1.382	17.76	81.9	20.1	28.8
2	1.74	104	1.382	17.76	81.9	20.1	28.8
3	1.73	125	1.373	18.02	81.9	20.3	29.1
4	1.74	104	1.382	17.76	81.9	20.1	29.1
5	1.75	87	1.390	17.50	82.0	19.9	29.2
6	1.73	125	1.373	18.02	81.9	20.3	29.4
7	1.72	153	1.363	18.28	81.8	20.4	29.8
8	1.70	233	1.343	18.81	81.6	20.6	30.7
9	1.72	153	1.363	18.28	81.8	20.4	31.2
10	1.70	233	1.343	18.81	81.6	20.6	31.5
11	1.69	286	1.333	19.08	81.6	20.7	32.2
12	1.68	342	1.325	19.36	81.5	20.9	32.6
13	1.68	342	1.325	19.36	81.5	20.9	32.7
14	1.66	500	1.307	19.90	81.3	21.1	34.3
15	1.66	500	1.307	19.90	81.3	21.1	34.5

Table S5. Summary of parameters for the optimistic singlet fission photon multiplier and the resulting solar cell for different fwhm calculated at standard test conditions. The optimistic case assumes 200 meV entropy gain, 3% parasitic absorption losses below the singlet fission band gap, capture losses of 5%, and a fwhm for the QD emission of 30 meV.

fwhm (meV)	$E(S_1)$ (eV)	E(QD) (eV)	V_{OC} (V)	J_{SC} (mA/cm^2)	FF (%)	η (%)
10	2.22	1.21	0.742	49.94	85.0	31.5
20	1.24	1.22	0.742	49.81	85.0	31.4
30	1.24	1.22	0.742	49.63	85.0	31.3
40	2.26	1.23	0.742	49.40	85.0	31.1
50	2.26	1.23	0.741	49.16	85.0	30.9

Table S6. Summary of parameters for the realistic singlet fission photon multiplier and the resulting solar cell for different fwhm calculated at standard test conditions. The realistic case assumes 100 meV entropy gain, 5% parasitic absorption losses below the singlet fission band gap, capture losses of 15%, and a fwhm for the QD emission of 30 meV.

fwhm (meV)	$E(S_1)$ (eV)	E(QD) (eV)	V_{OC} (V)	J_{SC} (mA/cm^2)	FF (%)	η (%)
10	2.32	1.21	0.740	46.31	84.9	29.0
20	2.34	1.22	0.740	46.23	84.9	29.0
30	2.34	1.22	0.740	46.10	84.9	29.0
40	2.36	1.23	0.740	45.94	84.9	28.9
50	2.36	1.23	0.740	45.76	84.9	28.7

Table S7. Linear fitting parameters for the efficiency of the two singlet fission photon multipliers and the tandem solar cell as a function of the silicon solar cell efficiency under standard test conditions.

	Offset	Slope
Realistic photon multiplier	-1.20	1.14
Optimistic photon multiplier	-2.12	1.26
Tandem solar cell	20.32	0.46

Table S8. Linear fitting parameters for the efficiency of the two singlet fission photon multipliers and the tandem solar cell as a function of the silicon solar cell efficiency under real-world conditions calculated using solar spectra and temperatures measured in Utrecht, The Netherlands.[21]

	Offset	Slope
Realistic photon multiplier	-0.96	1.13
Optimistic photon multiplier	-1.62	1.25
Tandem solar cell	17.00	0.48

Table S9. Linear fitting parameters for the efficiency of the two singlet fission photon multipliers and the tandem solar cell as a function of the silicon solar cell efficiency under real-world conditions calculated using solar spectra and temperatures measured in Denver, Colorado (US).[22]

	Offset	Slope
Realistic photon multiplier	-1.02	1.14
Optimistic photon multiplier	-1.38	1.21
Tandem solar cell	18.13	0.47

S5 THE EFFECT OF APE ON THE EFFICIENCY

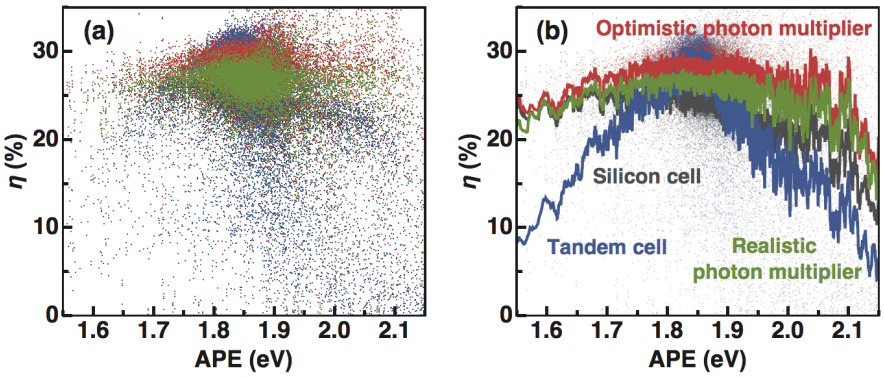

Figure S6. Efficiency of the two singlet fission photon multipliers, the tandem solar cell, and the silicon base cell as a function of average photon energy (APE) using solar spectra and temperatures measured in The Netherlands and in Colorado with the record silicon base cell with an efficiency of 27.6%.[21,22] The APE is calculated for photons with an energy above the band gap of silicon. The solid line in **(b)** represents a moving average of the data shown in **(a)**.

S6 DIFFERENT TANDEM SOLAR CELL CONFIGURAITONS

To compare the efficiency potential of the current-matched series tandem, the voltage-matched module tandem, and the electrically-independent four-terminal tandem we calculate the efficiencies of the three tandem configurations for different silicon bottom cells following previous work.[1] To optimize for maximum perovskite/silicon tandem solar cell efficiency, we change the band gap of the perovskite solar cell artificially by scaling the EQE of the record perovskite solar cell in energy while keeping the parasitic resistances and the electroluminescent emission efficiency constant. For the module tandem, we furthermore change ratio between the number of perovskite top cells and Si bottom cells to archive voltage-matching. Figure S7 shows the efficiencies of the different tandem cells as a function of the silicon-base-cell efficiency under standard test conditions and under real-world conditions. Both the module tandem and the four-terminal tandem are somewhat less

sensitive to changes in the solar spectrum than the series tandem. The average intensity-weighted efficiency of the module tandem and the four-terminal tandem is reduced by 2% in Colorado and by 3% in The Netherlands due to real-world conditions, while the efficiency of the series tandem cell is reduced by 3% in Colorado and by 4% in The Netherlands. Table S10, Table S11, and Table S12 show the fitting parameters to Figure S7.

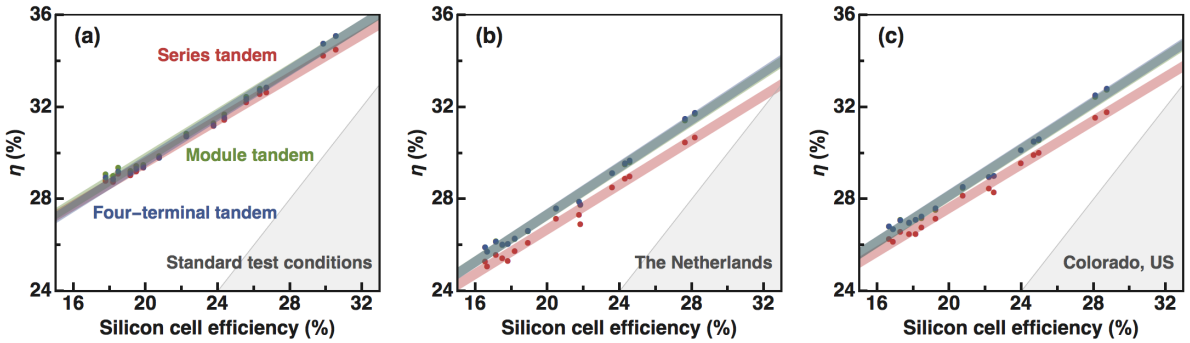

Figure S7. Efficiency of the tandem solar cells as a function of the silicon base cell efficiency under **(a)** standard test conditions and under real-world conditions averaged over the entire year and weighted with the incoming intensity, calculated using solar spectra and temperatures measured in **(b)** The Netherlands and **(c)** Colorado.[21,22]

Table S10. Linear fitting parameters for the efficiency of the three tandem solar cell configurations as a function of the silicon solar cell efficiency under standard test conditions.

	Offset	**Slope**
Series tandem	20.32	0.46
Module tandem	20.11	0.48
Four-terminal tandem	19.78	0.49

Table S11. Linear fitting parameters for the efficiency of the three tandem solar cell configurations as a function of the silicon solar cell efficiency under real-world conditions calculated using solar spectra and temperatures measured in Utrecht, The Netherlands.[21]

	Offset	Slope
Series tandem	17.00	0.48
Module tandem	17.11	0.51
Four-terminal tandem	17.02	0.52

Table S12. Linear fitting parameters for the efficiency of the three tandem solar cell configurations as a function of the silicon solar cell efficiency under real-world conditions calculated using solar spectra and temperatures measured in Denver, Colorado (US).[22]

	Offset	Slope
Series tandem	18.13	0.47
Module tandem	18.16	0.50
Four-terminal tandem	18.09	0.51

REFERENCES

(1) Futscher, M. H.; Ehrler, B. Modeling the Performance Limitations and Prospects of Perovskite/Si Tandem Solar Cells under Realistic Operating Conditions. *ACS Energy Lett.* **2017**, *2* (9), 2089–2095 DOI: 10.1021/acsenergylett.7b00596.

(2) Rau, U. Reciprocity Relation between Photovoltaic Quantum Efficiency and Electroluminescent Emission of Solar Cells. *Phys. Rev. B - Condens. Matter Mater. Phys.* **2007**, *76* (8), 1–8 DOI: 10.1103/PhysRevB.76.085303.

(3) Yoshikawa, K.; Kawasaki, H.; Yoshida, W.; Irie, T.; Konishi, K.; Nakano, K.; Uto, T.; Adachi, D.; Kanematsu, M.; Uzu, H.; et al. Silicon Heterojunction Solar Cell with Interdigitated Back Contacts for a Photoconversion Efficiency over 26%. *Nat. Energy* **2017**, *2*, 17032 DOI: 10.1038/nenergy.2017.32.

(4) Burkhard, G. F.; Hoke, E. T.; McGehee, M. D. Accounting for Interference, Scattering,

and Electrode Absorption to Make Accurate Internal Quantum Efficiency Measurements in Organic and Other Thin Solar Cells. *Adv. Mater.* **2010**, *22* (30), 3293–3297 DOI: 10.1002/adma.201000883.

(5) Yang, L.; Tabachnyk, M.; Bayliss, S. L.; Böhm, M. L.; Broch, K.; Greenham, N. C.; Friend, R. H.; Ehrler, B. Solution-Processable Singlet Fission Photovoltaic Devices. *Nano Lett.* **2014**, *15* (1), 354–358 DOI: 10.1021/nl503650a.

(6) Ehrler, B.; Wilson, M. W. B.; Rao, A.; Friend, R. H.; Greenham, N. C. Singlet Exciton Fission-Sensitized Infrared Quantum Dot Solar Cells. *Nano Lett.* **2012**, *12* (2), 1053–1057 DOI: 10.1021/nl204297u.

(7) Green, M. A.; Keevers, M. J. Optical Properties of Intrinsic Silicon at 300 K. *Prog. Photovoltaics Res. Appl.* **1995**, *3* (3), 189–192 DOI: 10.1002/pip.4670030303.

(8) Gao, L.; Lemarchand, F.; Lequime, M. Exploitation of Multiple Incidences Spectrometric Measurements for Thin Film Reverse Engineering. *Opt. Express* **2012**, *20* (14), 15734–15751 DOI: 10.1364/OE.20.015734.

(9) Yang, W. S.; Noh, J. H.; Jeon, N. J.; Kim, Y. C.; Ryu, S.; Seo, J.; Seok, S. Il. High-Performance Photovoltaic Perovskite Layers Fabricated through Intramolecular Exchange. *Science* **2015**, *348*, 235–1237 DOI: 10.1126/science.aaa9272.

(10) Futscher, M. H.; Ehrler, B. Efficiency Limit of Perovskite/Si Tandem Solar Cells. *ACS Energy Lett.* **2016**, *1*, 863–868 DOI: 10.1021/acsenergylett.6b00405.

(11) Green, M. A.; Emery, K.; Hishikawa, Y.; Warta, W.; Dunlop, E. D. Solar Cell Efficiency Tables (Version 38). *Prog. Photovoltaics Res. Appl.* **2011**, *19* (5), 565–572 DOI: 10.1002/pip.1150.

(12) Green, M. A.; Emery, K.; Hishikawa, Y.; Warta, W.; Dunlop, E. D. Solar Cell Efficiency Tables (Version 39). *Prog. Photovoltaics Res. Appl.* **2012**, *20* (1), 12–20 DOI: 10.1002/pip.2163.

(13) Green, M. A.; Emery, K.; Hishikawa, Y.; Warta, W.; Dunlop, E. D. Solar Cell Efficiency Tables (Version 40). *Prog. Photovoltaics Res. Appl.* **2012**, *20* (5), 606–614 DOI: 10.1002/pip.2267.

(14) Green, M. A.; Emery, K.; Hishikawa, Y.; Warta, W.; Dunlop, E. D. Solar Cell Efficiency Tables (Version 47). *Progress in Photovoltaics: Research and Applications*. Wiley-Blackwell January 2016, pp 3–11.

(15) Green, M. A.; Emery, K.; Hishikawa, Y.; Warta, W.; Dunlop, E. D. Solar Cell Efficiency

Tables (Version 48). *Prog. Photovoltaics Res. Appl.* **2016**, *24* (7), 905–913 DOI: 10.1002/pip.2788.

(16) Green, M. A.; Emery, K.; Hishikawa, Y.; Warta, W.; Dunlop, E. D.; Levi, D. H.; Ho-Baillie, A. W. Y. Solar Cell Efficiency Tables (Version 49). *Prog. Photovoltaics Res. Appl.* **2017**, *25* (1), 3–13 DOI: 10.1002/pip.2855.

(17) Green, M. A.; Emery, K.; Hishikawa, Y.; Warta, W.; Dunlop, E. D. Solar Cell Efficiency Tables (Version 45). *Prog. Photovoltaics Res. Appl.* **2015**, *23* (1), 1–9 DOI: 10.1002/pip.2573.

(18) Green, M. A.; Emery, K.; Hishikawa, Y.; Warta, W.; Dunlop, E. D. Solar Cell Efficiency Tables (Version 51). *Prog. Photovolt. Res. Appl.* **2012**, *26* (20), 12–20 DOI: 10.1002/pip.2978.

(19) Green, M. A.; Emery, K.; Hishikawa, Y.; Warta, W.; Dunlop, E. D. Solar Cell Efficiency Tables (Version 44). *Prog. Photovoltaics Res. Appl.* **2014**, *22* (7), 701–710 DOI: 10.1002/pip.2525.

(20) Green, M. A.; Hishikawa, Y.; Warta, W.; Dunlop, E. D.; Levi, D. H.; Hohl-Ebinger, J.; Ho-Baillie, A. W. H. Y.; Green, A. M.; Hishikawa, Y.; Wilhelm, W.; et al. Solar Cell Efficiency Tables (Version 50). *Prog. Photovoltaics Res. Appl.* **2017**, *25*, 668–676 DOI: 10.1002/pip.2909.

(21) van Sark, W. G. J. H. M.; Louwen, A.; de Waal, A. C.; Elsinga, B.; Schropp, R. E. I. UPOT: The Utrecht Photovoltaic Outdoor Test Facility. In *27th European Photovoltaic Solar Energy Conference and Exhibition*; WIP, 2012; pp 3247–3249.

(22) Stoffel, T.; Andreas, A. *NREL Solar Radiation Research Laboratory (SRRL): Baseline Measurement System (BMS); Golden, Colorado (Data)*; 1981.